ANALYTICAL SCIENCES MARCH 2020, VOL. 36

Rapid Communications

Toluene-sensing Properties of Mixed-potential Type Yttria-stabilized Zirconia-based Gas Sensors Attached with Thin CeO_2-added Au Electrodes

Nobumitsu OIDE, Taro UEDA, Kai KAMADA, Takeo HYODO, and Yasuhiro SHIMIZU†

Graduate School of Engineering, Nagasaki University, 1-14 Bunkyo-machi, Nagasaki 852–8521, Japan

Toluene-sensing properties of mixed-potential type yttria-stabilized zirconia (YSZ)-based sensors attached with a thin CeO_2-added Au sensing electrode (SE, CeO_2 content: 4 – 16 mass%, thickness: 30 – 100 nm), which was fabricated by using a spin-coating method, were examined and the effects of their SE thickness and the additive amount of CeO_2 on their toluene response were discussed in this study. The toluene response of the sensors attached with a 16 mass% CeO_2-added Au SE increased with an increase in the SE thickness, and the sensor attached with the thickest 16 mass% CeO_2-added Au SE showed the largest response, among all the sensors tested. This behavior probably arises from the increase in the number of active sites for electrochemical toluene oxidation in the CeO_2-added Au SE.

Keywords Solid-electrolyte gas sensor, mixed potential, Au, CeO_2, toluene

(Received January 28, 2020; Accepted January 30, 2020; Advance Publication Released Online by J-STAGE February 7, 2020)

Introduction

The exhaled breath of patients contains higher concentrations of specific gases than that of healthy people. For example, the patients suffering from lung cancer, diabetes and periodontitis release high concentrations of toluene, acetone and hydrogen sulfide, respectively.[1-4] Among various kinds of gas sensors, solid-electrolyte gas sensors have shown enhanced sensing properties to volatile organic compounds (VOCs) and volatile sulfide compounds (VSCs) by optimizing the microstructure and composition of sensing electrodes (SEs).[5,6] Especially, a Au-based SE mixed with metal oxides is one of the potential candidates for detecting VOCs and VSCs sensitively.[6-9] Zosel *et al.*, for example, reported that yttria-stabilized zirconia (YSZ)-based sensors equipped with a Au-based SE mixed with Nb_2O_5, Ga_2O_3, or In_2O_3 showed enhanced propylene response, as compared with that equipped with a pristine Au SE.[6] Elumalai *et al*. demonstrated that YSZ-based sensors equipped with a NiO-added Au SE could sensitively detect propylene.[9]

We have also examined seven kinds of rare-earth oxides as an additive to a Au SE of YSZ-based gas sensors, and reported that the addition of CeO_2 to the thick Au SE increased the toluene response.[10] This is probably due to an increase in the electrochemical activities for toluene oxidation at triple phase boundaries (TPBs, SE/YSZ/Gas) as a gas reaction site. On the other hand, the increase in the catalytic toluene oxidation activity decreased the toluene concentration around the TPBs at the interface between SE and YSZ and thus reduced the toluene response. Therefore, we focused on both the decrease in the thickness of the Au SE and the increase in the amount of CeO_2 dispersed uniformly into the Au SE. In addition, several researchers suggested that an increase in the number of the SE/YSZ interfaces with an increase in the roughness of the YSZ substrate improved the sensor responses to NO_2.[11-14] Since CeO_2 shows ionic conductivity,[15] the CeO_2-added Au works as a mixed ionic-electric conductor when their mixing state is optimized. Therefore, the interfaces between the CeO_2-added Au and gas (double phase boundaries (DPBs)) can electrochemically oxidize toluene, which leads to an increase in the toluene response. In this study, we fabricated 4 – 16 mass% CeO_2-added Au SEs with controlled thickness (30 – 100 nm) on YSZ by a spin-coating method, and investigated their toluene-sensing properties to clarify the effects of their SE thickness and the additive amount of CeO_2 on the toluene response.

Experimental

CeO_2-added Au SEs were fabricated by a spin-coating method. The coating solution was prepared by the addition of $Ce(NO_3)_3{\cdot}6H_2O$ and polyvinyl alcohol (PVA, number average molecular weight (Mn): 2400) into a 0.1 M $HAuCl_4$ aqueous solution. The solution was dropped on the YSZ (ZrO_2 doped with 8 mol% Y_2O_3, Japan Fine Ceramics Co., Ltd.) substrate (12×12 mm^2 in area, 0.5 mm in thickness), and then it was spun at 3000 rpm for 30 s, followed by heat treatment at 300°C for 5 min in air. This process was repeated multiple times to increase the film thickness. Then, they were annealed at 700°C for 2 h in air. The obtained sensing electrodes were denoted as $n$$CeO_2$/Au($t$) SEs ($n$: an additive amount of CeO_2, 4, 8, 16 (mass%); t: thickness of the SEs, 30, 60, 100 (nm)). A Pt paste was applied on the backside of the YSZ substrate by a screen-printing method, and then it was annealed at 700°C for 2 h in air, to fabricate the counter electrode (CE; 4×1 mm^2 in area, *ca*. 11 μm in thickness). The fabricated sensor ($n$$CeO_2$/Au($t$) sensor) was attached to a mullite tube (Nikkato Corp.) with an inorganic adhesive, as shown in Fig. 1. It was mounted in the tubular furnace, and then response properties of the sensors to

† To whom correspondence should be addressed.
E-mail: shimizu@nagasaki-u.ac.jp

50 ppm (parts per million in volume) toluene in dry air were measured in a flow apparatus (gas-flow rate: 10^{-4} m^3 min^{-1}) at 500°C. The electromotive force (E, mV) of the sensors as a sensing signal was measured with a digital electrometer (Keysight Technologies, Inc., 34970A) and the response (ΔE) was defined as the difference in E between in dry air and in toluene balanced with dry air. The microstructural images of the Au SEs were obtained by scanning electron microscopy (SEM; JEOL Ltd., JSM-5700).

Results and Discussion

Cross-sectional SEM images of *4*CeO_2/Au(*t*) SEs are shown in Figs. 2a – 2c. The electrode thickness of the *4*CeO_2/Au(*30*) SE, which was fabricated by 5-time spin coating, was very thin (*ca.* 30 nm), and the thickness increased with an increase in the number of spin-coating cycles. Namely, the thickness of the SEs was controlled from 30 to 100 nm only by changing the number of spin-coating cycles. A SEM image of the *4*CeO_2/Au(*30*) SE surface is shown in Fig. 2d. A large number of highly CeO_2-dispersive Au agglomerates (100 – 500 nm in size) covered the YSZ surface homogeneously and there were various voids among the boundaries of their agglomerates. We have already reported that submicron-sized CeO_2 particles were microstructurally separated with Au, but the CeO_2 particles were relatively dispersed in a thick Au SE (thickness: *ca.* 10 µm) when a Au paste mixed with the CeO_2 particles was directly screen-printed on a YSZ substrate.[10] Compared with its microstructure and the thickness, the spin-coating method using their raw materials ($HAuCl_4$ and $Ce(NO_3)_3{\cdot}6H_2O$) with PVA was obviously a quite effective way to fabricate thinner *4*CeO_2/Au(*t*) SEs with more dispersive CeO_2 particles.

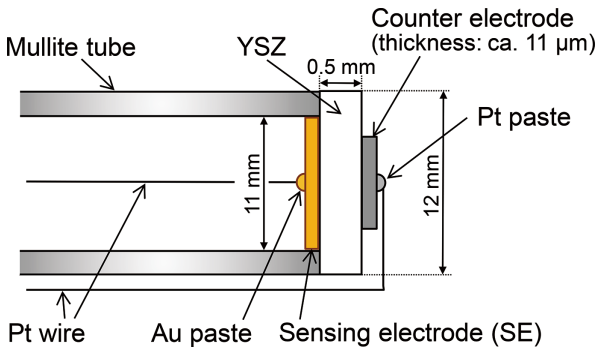

Fig. 1 Schematic view of a *n*CeO_2/Au(*t*) sensor.

Response transients of the *n*CeO_2/Au(*t*) sensors to 50 ppm toluene at 500°C in dry air are shown in Figs. 3a – 3c, and variations in the toluene response (ΔE) of their sensors with the thickness of the SEs (t) are shown in Fig. 3d. The E values of all the sensors negatively shifted upon exposure to toluene, but ΔE was largely affected by the SE thickness and the additive amount of CeO_2. Generally, the VOC-sensing mechanism of solid-electrolyte gas sensors, as discussed in various papers, can be explained on the basis of the mixed potential theory.[16-18] The effects of the thickness of SEs and the amount of CeO_2 in SEs on toluene oxidation in SEs are schematically summarized in Fig. 4. The electrochemical oxidation of toluene (Eq. (1)) and

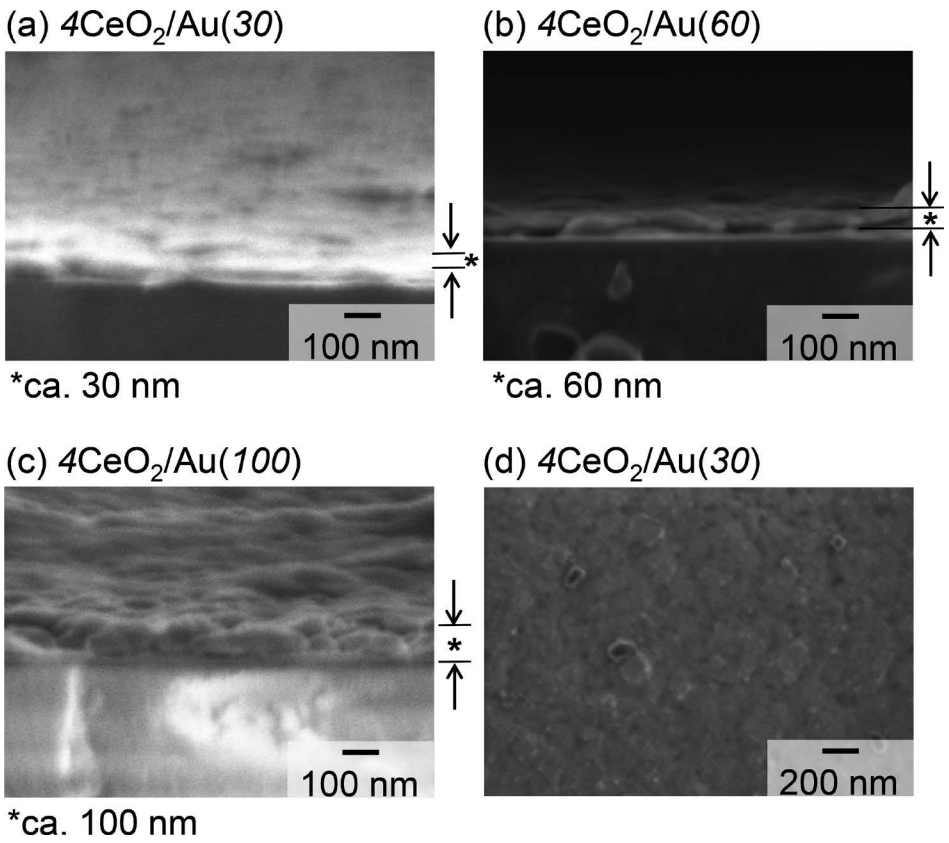

Fig. 2 SEM images of (a – c) cross-section of *4*CeO_2/Au(*t*) SEs and (d) surface of a *4*CeO_2/Au(*30*) SE. *: Thickness of *4*CeO_2/Au(*t*) SEs.

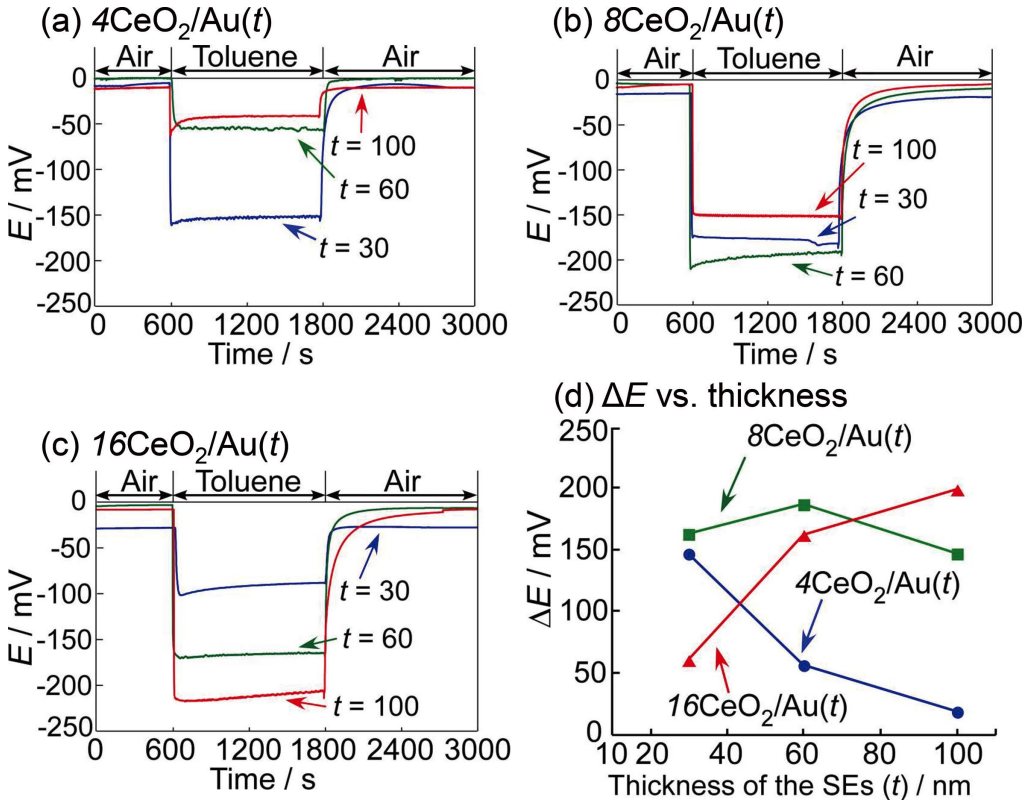

Fig. 3 (a – c) Response transients of nCeO$_2$/Au(t) sensors to 50 ppm toluene at 500°C in dry air, and (d) variation in response of the nCeO$_2$/Au(t) sensors to 50 ppm toluene at 500°C in dry air with thickness of the SEs (t).

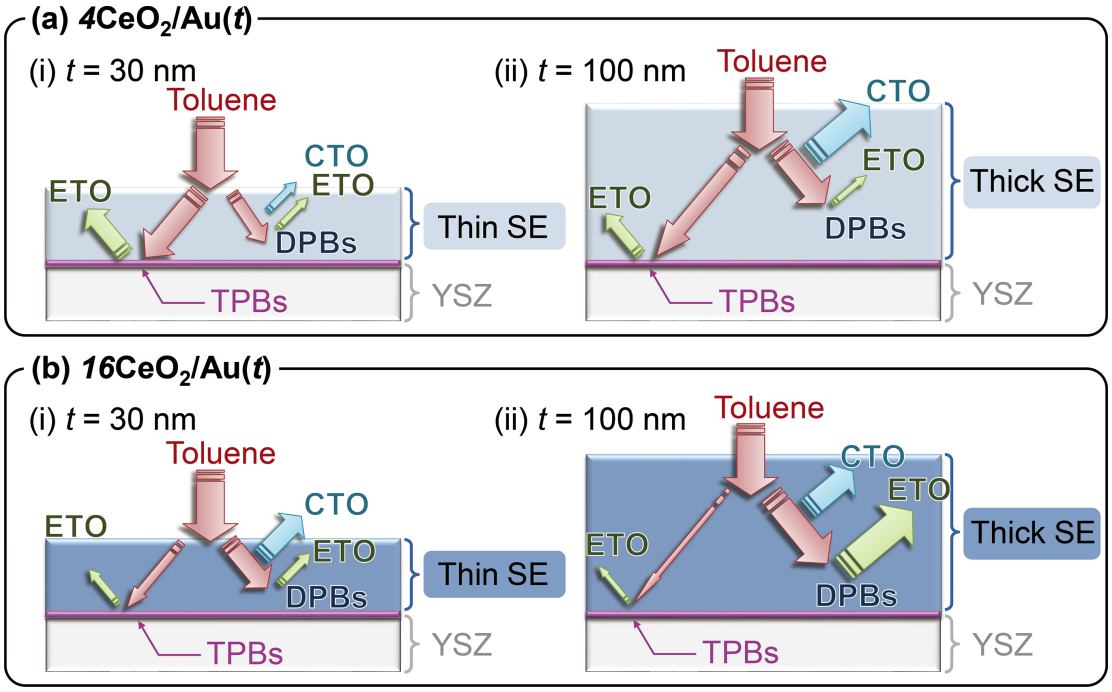

Fig. 4 Schematic views of the contribution of both CTO sites in SEs and ETO sites (DPBs in SEs and TPBs at SE/YSZ interface (pinkish line)) to toluene responses of nCeO$_2$/Au(t) sensors. Thickness of the red arrows shows the concentration of toluene that reached these sites, while that of the blue and green arrows shows the concentration of various products (mainly, carbon dioxide and water) produced at CTO sites and ETO sites, respectively. CTO: catalytic toluene oxidation, ETO: electrochemical toluene oxidation, TPBs: triple phase boundaries, and DPBs: double phase boundaries.

electrochemical reduction of oxygen (Eq. (2)) simultaneously proceed at TPBs at the interface between SE and YSZ, when toluene diffuses in SE and reaches TPBs. At that time, the *E* values are determined by these reactions which simultaneously proceed at the same rate at TPBs.

$$C_7H_8 + 18O^{2-} \longrightarrow 7CO_2 + 4H_2O + 36e^- \quad (1)$$

$$O_2 + 4e^- \longrightarrow 2O^{2-} \quad (2)$$

We previously reported the *I*–*E* characteristics of the sensors attached with a pristine Au SE and a 4 mass% CeO_2-added Au SE fabricated by screen printing. The absolute value of the net anodic current of toluene oxidation of the sensor attached with a CeO_2-added Au SE was much larger than that with a pristine Au SE,[11] which indicated an increase in the electrochemical toluene oxidation (ETO) activity by the addition of CeO_2 at TPBs, leading to the enhanced ΔE of the *n*CeO_2/Au(SP) sensor (SP: screen printing, thickness of the *n*CeO_2/Au(SP) SE: *ca.* 10 μm).[11] In addition, a certain amount of toluene is catalytically oxidized at catalytic toluene oxidation (CTO) sites, which are probably on the CeO_2 surface, during the diffusion in SE. Therefore, the actual concentration of toluene at TPBs decreased with an increase in the SE thickness, namely an increase in the number of CTO sites, and thus the amount of ETO on TPBs became reduced, as shown in Fig. 4a. In addtion, CeO_2 shows ionic conductivity,[15] and thus the CeO_2-added Au works as a mixed ionic-electric conductor. Therefore, we can consider that ETO easily proceeds at the interfaces between the CeO_2-added Au and gas (DPBs). We already reported that the *4*CeO_2/Au(SP) sensor also showed rather high toluene response (ΔE: *ca.* 130 mV),[11] but ΔE of the *4*CeO_2/Au(*30*) sensor (*ca.* 150 mV) was slightly larger than that of the *4*CeO_2/Au(SP) sensor. This is probably because the toluene concentration at TPBs of the *4*CeO_2/Au(*30*) sensor having a thinner SE (*ca.* 30 nm) was larger than that of the *4*CeO_2/Au(SP) sensor having a thicker SE (*ca.* 10 μm), even though the microstructure of the *4*CeO_2/Au(*30*)SE was denser than that of the *4*CeO_2/Au(SP) SE and thus the relatively slow gas-diffusion rate in the *4*CeO_2/Au(*30*) SE expectedly reduced the toluene concentration at TPBs.

However, ΔE of the *4*CeO_2/Au(*t*) sensors largely decreased with an increase in the thickness of SEs, and resulted in much smaller ΔE of the *4*CeO_2/Au(*100*) sensor in comparison with that of the *4*CeO_2/Au(SP) sensor. This fact explained the slow gas-diffusion rate in the *4*CeO_2/Au(*t*) SE, and the large amount of toluene catalytically oxidized at CTO sites. Since the addition of CeO_2 into the Au SEs increased ETO activity at TPBs, ΔE of the *8*CeO_2/Au(*30*) sensor was larger than that of the *4*CeO_2/Au(*30*) sensor. On the other hand, ΔE of the *16*CeO_2/Au(*t*) sensors increased with an increase in the thickness of SEs, and the *16*CeO_2/Au(*100*) sensor showed the largest ΔE (*ca.* 199 mV) among the sensors examined. Thus, the incease in ΔE of the *16*CeO_2(*t*) sensors with an increase in the thickness can be explained by the contribution of DPBs to ETO (compare Fig. 4b). One of possible explanations is that the contribution of DPBs to ETO is more effective than that of TPBs, because the actual concentration of toluene on the upper part of SE should be higher than that on the bottom part, as menthined above. Thus, the toluene response of the *16*CeO_2/Au(*t*) sensors is determined by the ETO activity at DPBs. Another one is that an increase in the number of electrochemical reaction sites (both DPBs and TPBs) contributed to an increase in ΔE. However, the *16*CeO_2/Au(*30*) sensor showed the smallest ΔE among the *n*CeO_2/Au(*30*) sensors. This is probably because the amount of toluene reaching the TPBs at the SE/YSZ interface decreased with an increase in the number of CTO sites during gas diffusion in SE. In addition, the contribution of ETO at DPBs to the toluene response is also low due to the small number of electrochemical reaction sites at DPBs (compare Fig. 4ai and Fig. 4bi). Although the detailed mechanism of this phenomena should be examined in the future, the existence of DPBs in SEs largely contributes to an increase in the toluene response, in this study. The fact that the ΔE of the *8*CeO_2/Au(*60*) sensor was the largest among the *8*CeO_2/Au(*t*) sensors can be explained by the contribution of ETO consisting of DPBs and TPBs together with CTO. We now believe that the microstructural optimization of SEs and the strict control of the additive amount of CeO_2 into SEs succeed in further improving the toluene response of the *n*CeO_2/Au(*t*) sensors.

Acknowledgements

This work was supported by the Japan Society for the Promotion of Science (JSPS) KAKENHI Grant Number 19K05005.

References

1. W.-T. Koo, S.-J. Choi, N.-H. Kim, J.-S. Jang, and I.-D. Kim, *Sens. Actuators, B*, **2016**, *223*, 3010.
2. K. Yaegaki and K. Sanada, *J. Periodont. Res.*, **1992**, *27*, 233.
3. W. Li, W. Dai, M. Liu, Y. Long, C. Wang, S. Xie, Y. Liu, Y. Zhang, Q. Shi, X. Peng, Y. Liu, Q. Li, and Y. Duan, *BMJ Open.*, **2019**, e028448.
4. R. Kalidoss and S. Umapathy, *Biomed. Microdevices*, **2020**, *22*, 2.
5. X. Hao, C. Ma, X. Yang, T. Liu, B. Wang, F. Liu, X. Liang, C. Yang, H. Zhu, and G. Lu, *Sens. Actuators, B*, **2018**, *255*, 3033.
6. J. Zosel, D. Westphal, S. Jakobs, R. Müller, and U. Guth, *Solid State Ion.*, **2002**, *152*, 525.
7. S. Thiemann, R. Hartung, U. Guth, and U. Schonauer, *Ionics*, **1996**, *2*, 463.
8. T. Hibino, S. Kakimoto, and M. Sano, *J. Electrochem. Soc.*, **1999**, *146*, 3361.
9. P. Elumalai, V. V. Plashnitsa, Y. Fujio, and N. Miura, *Sens. Actuators, B*, **2010**, *144*, 215.
10. T. Ueda, H. Abe, K. Kamada, S. R. Bishop, H. L. Tuller, T. Hyodo, and Y. Shimizu, *Sens. Actuators, B*, **2017**, *252*, 268.
11. R. Sun, Y. Guan, X. Cheng, Y. Guan, X. Liang, J. Ma, P. Sun, Y. Sun, and G. Lu, *Sens. Actuators, B*, **2015**, *210*, 91.
12. X. Liang, S. Yang, J. Li, H. Zhang, Q. Diao, W. Zhao, and G. Lu, *Sens. Actuators, B*, **2011**, *158*, 1.
13. Y. Guan, C. Li, X. Cheng, B. Wang, R. Sun, X. Liang, J. Zhao, H. Chen, and G. Lu, *Sens. Actuators, B*, **2014**, *198*, 110.
14. X. Cheng, C. Wang, B. Wang, R. Sun, Yi. Guan, Y. Sun, X. Liang, P. Sun, and G. Lua, *Sens. Actuators, B*, **2015**, *221*, 1321.
15. R. Gerhardt-Anderson and A. S. Nowick, *Solid State Ion.*, **1981**, *2*, 547.
16. T. Kida, N. Morinaga, S. Kishi, K. An, K. Sim, B. Chae, J. Kim, B. Ryu, and K. Shimanoe, *Electrochim. Acta*, **2011**, *56*, 7484.
17. N. Miura, T. Sato, S. A. Anggraini, H. Ikeda, and S. Zhuiykov, *Ionics*, **2014**, *20*, 901.
18. F. Liu, Z. Yang, J. He, R. You, J. Wang, S. Li, H. Lu, X. Liang, P. Sun, X. Yan, X. Chuai, and G. Lu, *Sens. Actuators, B*, **2018**, *272*, 433.